Atmospheric Environment 244 (2021) 117992

Contents lists available at ScienceDirect

Atmospheric Environment

journal homepage: http://www.elsevier.com/locate/atmosenv

Differential inflammatory potential of particulate matter (PM) size fractions from imperial valley, CA

S.M. D'Evelyn [a,*], C.F.A. Vogel [a,b], K.J. Bein [a], B. Lara [c], E.A. Laing [a], R.A. Abarca [a], Q. Zhang [b], L. Li [b], J. Li [b], T.B. Nguyen [b], K.E. Pinkerton [a]

[a] Center for Health and the Environment, University of California, Davis, USA
[b] Department of Environmental Toxicology, University of California, Davis, USA
[c] KBI Biopharma, Inc., Boulder, CO, USA

HIGHLIGHTS

- PM size fractions have distinct chemical compositions.
- PM_{10} triggers a distinct biological response compared to smaller particles.
- PM_{10} triggers an inflammatory response in macrophages.
- Exposure to ultrafine and $PM_{2.5}$ activates the aryl hydrocarbon receptor.

ARTICLE INFO

Keywords:
Particulate matter
Coarse PM
Size fraction
Bioaerosols
Endotoxin
Imperial valley

ABSTRACT

Particulate matter (PM) in Imperial Valley originates from a variety of sources such as agriculture, traffic at the border crossing, emissions from the cross-border city of Mexicali, and the drying lakebed of the Salton Sea. Dust storms in Imperial Valley, California regularly lead to exceedances of the federal air quality standards for PM_{10} (diameter less than 10 μm). To determine if there are differences in the composition and biological response to Imperial County PM by size, ambient PM samples were collected from a sampling unit stationed in the northernmost part of the valley, South of the Salton Sea. Ultrafine, fine, and coarse PM samples were collected and extracted separately. Chemical composition of each size fraction was obtained after extraction by using several analytical techniques, and biological response was measured by exposing a cell line of macrophages to particles and quantifying subsequent gene expression. Biological measurements demonstrated coarse PM induced an inflammatory response in macrophages measured in increases of inflammatory markers *IL-1β, IL-6, IL-8* and *CXCL2 expression*, whereas ultrafine and fine PM only demonstrated significant increases in expression of *CYP1a1*. These differential responses were due not only to particle size, but to the distinct chemical profiles of each size faction as well. Community groups in Imperial Valley have already completed several projects to learn more about local air quality, giving residents access to data that provides real-time levels of $PM_{2.5}$ and PM_{10} as well as recommendations on health-based practices dependent on the current AQI (air quality index). However, to date there is no information on the composition or toxicity of ambient PM from the region. The data presented here could provide more definitive information on the toxicity of PM by size, and further inform the community on local air quality.

1. Introduction

Particulate matter (PM) is a heterogenous mix of solid and liquid particles suspended in the air. PM originates from a variety of sources, both anthropogenic and natural in origin. Ambient PM can vary in size, shape, charge and composition, as influenced by the surrounding environment, season, and even time of day (Mack et al., 2019). It is well known that exposure to excess levels of PM pollution can lead to cardiopulmonary and neurological health effects in both healthy and susceptible populations. Due to the complexity of PM, it is difficult to

* Corresponding author. One Shields Ave, Davis, CA, 95616, USA.
E-mail address: smack@ucdavis.edu (S.M. D'Evelyn).

https://doi.org/10.1016/j.atmosenv.2020.117992
Received 15 January 2020; Received in revised form 5 October 2020; Accepted 11 October 2020
Available online 14 October 2020

determine which of these characteristics leads to the observed adverse health effects.

PM is categorized into three main size fractions: coarse ($PM_{10-2.5}$, with aerodynamic diameter (D_a) > 2.5 μm, but < 10 μm), fine ($PM_{2.5-0.1}$, D_a = 0.1–2.5 μm), and ultrafine (UF, D_a < 0.1 μm). For the purposes of this paper, these fractions will be referred to as PM_{10}, $PM_{2.5}$ and ultrafine respectively (Mack et al., 2019). While size itself is a potential driver for health outcomes, it is impossible to completely separate particle size from its chemical composition. As reviewed by Kelly and Fussel (2012), $PM_{2.5}$ and ultrafine PM originate primarily from combustion emissions and gas-to-particle partitioning processes, whereas PM_{10} is primarily resuspended dust from crustal materials. PM_{10} can also include bioaerosols such as endotoxin, mold and fungal spores (Badirdast et al., 2017; Kelly and Fussell, 2012; Robertson et al., 2019; Samake et al., 2017). Ultrafine and $PM_{2.5}$ particles are often termed "respirable particles" due to their ability to easily enter the alveolar region of the lung (Madl et al., 2010). During nasal breathing, larger, inhalable particles are mostly captured in the upper respiratory tract; however, these larger particles can also be respired into the lungs during oral-breathing, such as during nasal congestion or exercise (Madl et al., 2010). As such, the effect of coarse particles (PM_{10}) should not be overlooked, especially where they are the dominant size fraction of total PM pollutant mass.

Imperial County is located in the southernmost part of California, immediately adjacent to the U.S.-Mexico border. This county consistently ranks as the region with one of the highest annual particulate pollution levels in the state of California (American Lung Association, 2019; California Air Resources Board, 2018). In recent years, Imperial County has also ranked as the county with the highest childhood asthma rate in California (Health, 2015-2017). PM in Imperial Valley (Fig. 1) comes from a wide variety of sources including, but not limited to, crop-based agriculture, cattle feedlots, idle vehicles at the border crossing, the megacity of Mexicali, and the exposed lakebed of the evaporating Salton Sea (Kelly et al., 1995). As agricultural and industrial runoffs are the Salton Sea's only inflow source, the sea is becoming increasingly polluted and is rapidly shrinking (Frie et al., 2017). Potentially toxic particles arising from the crustal, dry lakebed of the Salton Sea are unique to the region and are a prominent source of PM_{10} (Frie et al., 2017).

In order to determine if there are differences in the composition of as well as the biological response to Imperial County PM, ambient PM samples of three different size fractions were collected from a sampling unit stationed just south of the Salton Sea. We hypothesize that due to an inherent difference in chemical composition, the biological response to each size fraction will be unique.

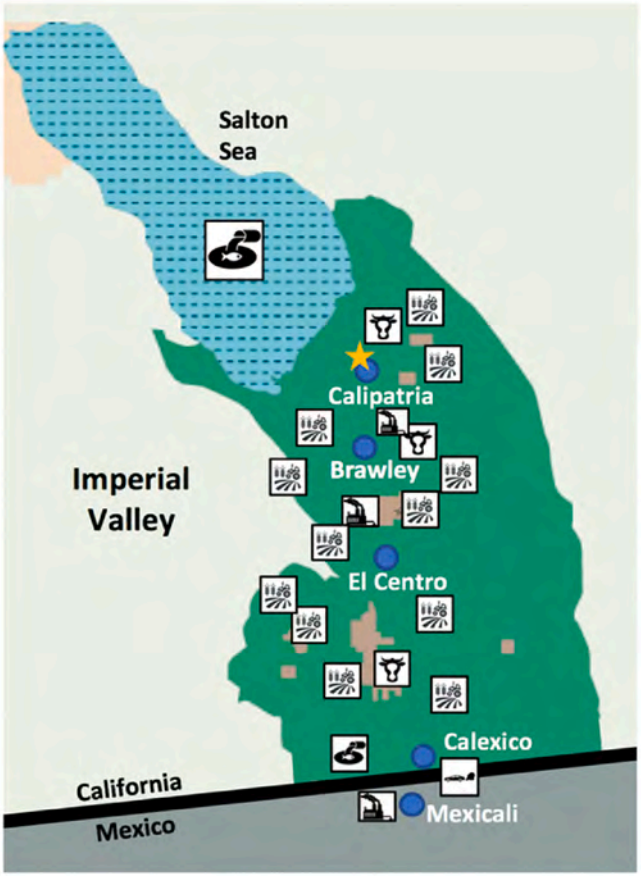

Fig. 1. Map of Imperial Valley with a selection of the main PM sources in the valley: polluted water, agricultural fields, cattle feedlots, factories, and the border crossing. The collection site of the sampling unit is marked with a star.

2. Methods

The sampling unit collected all three size fractions of PM, as well as meteorological and average air quality data, over the course of three weeks. Once collected, samples were chemically characterized and tested in an *in vitro* system to model the response when inhaled. As macrophages are the resident immune cells and primary responder in the lungs when a foreign object is inhaled and deposited, a cell line of macrophages was used to measure the biological response.

2.1. Sampling Site Selection

Sampling site selection criteria were based on several factors, including: 1) specific interest in windblown dust from the Salton Sea playa, 2) proximity to schools so sampled PM mixtures are representative of what children are actually exposed to, and students can be engaged in the research project, such as operational maintenance of the PM samplers and instrumentation described later, and 3) a location in the northern portion of the valley close to the Salton Sea and in alignment with the predominant wind directions so that major emission sources of interest, such as the Salton Sea playa, Mexicali, and surrounding agriculture, are routinely transported to the site. During reconnaissance, numerous sampling sites were vetted with the aid of several community stakeholders and a location on the Calipatria School District campus was ultimately chosen, which includes an elementary school, middle school and high school. The Salton Sea is to the north-northwest, Mexicali is to the south and the area is surrounded by agriculture and large livestock operations.

2.1.1. PM Sampling and Measurement Platform (PMSAMP)

A state-of-the-art, fully remote-controllable PM Sampling and Measurement Platform (PMSAMP) was deployed during this study to collect size-segregated PM samples and provide real-time measurements of air quality and meteorological parameters. Supplemental Figure 1 shows the PMSAMP deployed on the Calipatria School District campus. All size-segregated PM sampling was performed using ChemVol (CV) samplers (Demokritou et al., 2002), which are high flow rate (900 lpm), impactor-based samplers with multiple impactor stages that can be stacked in series to collect size-segregated PM for a range of size cuts. As shown in Supplemental Figure 1, the CV sampling train is housed inside the PMSAMP. Following the airflow, ambient air is drawn into an 8" diameter, 10-foot-tall sampling stack situated on top of the trailer, plumbed across the trailer roof and through the wall to the CV manifold, which houses 10 separate CV stacks. Each CV stack includes an after-filter support and 0.17, 1.0 and 2.5 μm stages. A single 10 μm stage is located upstream of the CV manifold. In this configuration, the ultrafine (D_p < 0.17 μm), submicron fine (0.17 < D_p < 1 μm), and

supermicron ($1 < D_p < 2.5$ μm) size fractions can be collected for each of the 10 CV stacks and a single PM_{10} sample is collected from the 10 μm stage. Ultrafine PM was collected on Teflon-bound borosilicate glass microfiber filters (Pallflex TX40) while all other PM size fractions were collected on polyurethane foam (PUF) substrates.

Computer-controlled solenoid valves are connected to the bottom of each CV stack and plumbed into a single manifold. Inserted downstream of the valve manifold is an industrial-scale inline thermal mass flow transmitter for monitoring flow rate. At the outlet of the flow meter, 2″ steel pipe leads out the trailer floor, followed by 20′ of 2″ rubber double-reinforced suction hose attached to the inlet of the blower assembly. The blower assembly includes a variable frequency drive with PID (proportional-integral-differential) feedback from the flow meter to power the blower and maintain the desired flowrate. In this configuration, the CV stacks can be computer controlled to operate in succession according to any sampling algorithm or protocol of interest. For example, different CV stacks can be programmed to operate at different times of day or when the wind originates from different directions. For the current study, four separate CVs were used to collect PM samples as a function of time of day: 00:00–06:00, 06:00–12:00, 12:00–18:00 and 18:00–24:00. This allowed for isolation of time periods when children are outside playing and most likely to be exposed to high levels of PM. The time period chosen for the current study was 12:00–18:00 and sampling was conducted for a three-week period during the summer 2018 (06/20/2018-07/10/2018).

Co-located instrumentation for monitoring air quality and meteorological conditions included: *(i)* a Scanning Mobility Particle Sizer providing 15 min resolution measurements of the size distribution of particle number concentration in the range 10–800 nm, *(ii)* two DustTrak monitors providing 15 s resolution measurements of $PM_{2.5}$ and PM_{10} mass concentration, *(iii)* high precision, solid state sonic wind direction and speed sensors providing 3 s resolution measurements of wind speed and direction, *(iv)* a meteorological station providing continuous ambient temperature, pressure, relative humidity and incoming solar radiation, (v) 10.6 eV photoionization detector (PID) for 10-s resolution measurements of volatile organic compounds with integrated electrochemical sensors for CO_2, CO and NO_2 and *(vi)* security cameras providing continuous 360° imaging of the sampling site and surrounding area. The air quality monitors are housed inside the PMSAMP while the wind speed and direction sensors, meteorological station and PID are mounted on poles extending from the roof, as shown in Supplemental Figure 1. A separate sampling stack, also shown in Supplemental Figure 1, is plumbed through the window to a sampling port manifold inside the PMSAMP. The downstream end of the sampling port is plumbed out the window and underneath the trailer to an inline blower. All air quality instruments sample from separate manifold ports. All instrumentation and sampling equipment are controlled by a custom-built computer and integrated custom software. Full remote control and surveillance capabilities are achieved via the internet using a mobile hot spot.

2.2. PM Extraction

For toxicological assessment and chemical characterization, PM collected on glass microfiber filters and PUF substrates underwent a multi-solvent extraction process to provide a dry PM extract. The extraction protocols have been described in detail by Bein and Wexler (2014). Due to extensive build-up of particles, PM_{10} was extracted by scraping particles from the surface of the PUF substrate using a sterilized metal spatula. Extracted particles were weighed as dry material using a microanalytical balance, and then resuspended in nanopure water to a concentration of 1 μg/μL (1 mg/mL) for use in *in vitro* experiments. . Separate aliquots of the dry PM extracts were used for all chemical analysis to ensure that toxicological assessment and chemical characterization were performed on identical samples.

2.3. PM Characterization

Chemical analyses were performed on the material extracted from the sample substrates as well as blank controls, similarly to those administered in the bioassays. A limitation of this study is the potential alteration of particles through the extraction process, including dissolution of soluble substances and particle agglomeration (Supplemental Table 1). However, particles collected using the high flow rate, impactor-based sampler are optimally size-separated. All extracted PM samples were divided into multiple aliquots of known PM mass concentration in solutions specific to the various analytical techniques used. Field blank extracts were divided into the same number of aliquots using identical solvent volumes as the PM extracts to ensure proper field blank correction. A process blank was also included for each method to quantify any potential sources of contamination during sample preparation.

2.3.1. Particle morphology was analyzed with micro-flow imaging (MFI)

Particle morphology was analyzed with micro-flow imaging (MFI) a sensitive, microscopy-based technique capable of counting and morphologically characterizing micro-scale particles. Bright-field particle images (≥1 μm) are captured as a solution passes through a flow cell. The detection method relies on changes in refractive indices which make it sensitive to translucent particles. The images collected are used by the software to create an extensive database of information (size, shape, transparency) that can be used to classify and differentiate the particles detected. The method has an upper limit of detection of 1 million particle images per analysis and 2 million particles/mL. Dilution, therefore, was required for the ultrafine and PM_{10} samples. Negative controls of water baselines were monitored throughout sample analyses to ensure cleanliness of the system (no more than 100 particles/mL ≥ 1 μm).

2.3.2. Trace metals

Trace metals were identified via Inductively Coupled Plasma-Mass Spectrometry (ICP-MS) according to standard methods of operation, along with calibration standards, QA/QC and MDL/error analyses through the Interdisciplinary Center for Plasma Mass Spectrometry at UC Davis. Due to the variability between PM samples, this methodology was selected due to the sensitivity of measurements down to femtomolar levels. The elements analyzed included Li, Be, Na, Mg, Al, K, Ca, V, Cr, Mn, Fe, Co, Ni, Cu, Zn, As, Se, Rb, Sr, Ag, Cd, Cs, Ba, Tl, Pb and U.

2.3.3. Water soluble inorganic and organic ions

Water soluble inorganic and organic ions were measured through Ion Chromatography (IC) according to the calibration standards, quality assurance, and error analyses protocols previously reported (Ge et al., 2014; Parworth et al., 2017). Analyzed ions include NH_4^+, F^-, Br^-, Cl^-, NO_2^-, NO_3^-, SO_4^{2-}, PO_4^{3-}, Li^+, Na^+, Mg^{2+}, K^+, Ca^{2+}, 9 deprotonated organic acids and 9 protonated amines. Sample preparation included dilution of the PM, field blank and process blank aliquots to a 10 mL volume, bath sonication, filtering using a 0.2 μm pore size and then refrigeration until analysis (within 12 h of sample preparation).

2.3.4. Total organic PM mass and composition

Total organic PM mass and composition was measured via high-resolution time-of-flight aerosol mass spectrometry (HRAMS) (Canagaratna et al., 2007; DeCarlo et al., 2006) according to previously reported protocols (Ge et al., 2014; Sun and Zhang, 2010). This approach has the advantage of using 70 eV electron impact mass spectrometry analysis, which is quantitative and does not suffer from matrix effects. It is also able to quantify the elemental composition of major ions, thus the average molar ratios among elements in organic PM, e.g., oxygen-to-carbon (O/C), nitrogen-to-carbon (N/C), sulfur-to-carbon (S/C), and hydrogen-to-carbon (H/C) (Aiken et al., 2007, 2008). Sample preparation included the resuspension of the extracted and

lyophilized PM, field blanks and process blank aliquots in nanopure water, sonication at ~ 0 °C for 1 h, and refrigeration until analysis (within 12 h of sample preparation). The molecular composition was also measured with high-resolution mass spectrometry (HRMS), using direct-infusion nanospray ionization coupled to a linear trap quadrupole (LTQ)-Orbitrap instrument (Thermo Electron Corp.) at a mass resolving power of 60,000 m/Δm at m/z 400 in the positive ion mode. An external calibration was performed immediately prior to analysis to achieve a mass accuracy of 2 ppm. Each ionizable compound in the sample was observed as protonated ([M+H]+ ions) and/or sodiated ([M+Na]+ ion. Mass spectra were processed by subtracting the background mass spectra of the blank filter extracts, deconvoluted and deisotoped, mass corrected, and assigned to molecular formulas using a custom Matlab protocol based on heuristic mass filtering rules (Kind and Fiehn, 2007) and Kendrick Mass (KM) defect analysis (Kendrick, 1963) with KM base of CH_2.

2.3.5. Elemental analysis

Elemental analysis was performed using Scanning Electron Microscopy/Energy Dispersive X-ray Spectroscopy (SEM-EDS) to provide topographical images of particles to understand their three-dimensional structure. This methodology includes qualitative particle identification through relative quantitative elemental analysis. Elemental analysis was performed on a blank filter and filter with collected PM_{10} particles. Reported elemental components of PM_{10} yielded FIT scores >0.9. A FIT score of 1.0 indicates a perfect match.

2.3.6. Bacterial endotoxins

Bacterial endotoxins were quantified with the Pierce Chromogenic Endotoxin Quant Kit (Catalog Number: A39552) with e.*coli* standard controls, following the Thermo Scientific Pierce protocol. All materials were heated overnight to reduce endotoxin contamination. Endotoxin-free water served as a blank control. This assay was performed on two aliquots of each size fraction (ultrafine, $PM_{2.5}$ and PM_{10}) of PM: one aliquot heated at 120 °*C* overnight before the assay to remove endotoxin, following a protocol modified from Wegesser et al. (Wegesser and Last, 2008).

2.3.7. β-glucans

ß-glucans were measured in PM samples to detect the presence of any fragments of fungal cell walls (Douwes, 2005; Wegesser and Last, 2008). The (1 → 3) Beta-D-glucan Glucatell assay is a modification of the Limulus Amebocyte Lysate (LAL) pathway that reacts with bacterial endotoxin but specific to (1 → 3) Beta-D-glucan. All materials were heated overnight at 235 °C to remove any interfering substances as recommended by the protocol of Glucatell CapeCod Associates (Catalog number: #GT004). This assay was performed using two aliquots of each size fraction (ultrafine, PM2.5 and PM10) of PM: one aliquot heated at 120 °C overnight before the assay.

2.4. PM in vitro exposure:

Cellular responses to PM were quantified by measuring gene expression levels with a panel of toxicity and inflammatory markers detected by quantitative real-time Reverse Transcription-Polymerase Chain Reaction (qRT-PCR). Reactive oxygen species (ROS) was measured using the stress response protein hemeoxygenase-1 (HO-1), inflammation via the cyclooxygenase-2 (COX-2), interleukin 1 beta, 6, 8 and 10 (IL-1β; IL-6; IL-8; IL-10) and chemokine ligand 2 (CXCL2) proteins, and polycyclic aromatic hydrocarbon (PAH) activation via cytochrome P450 1A1 (CYP1A1) expression (Lingappan et al., 2017).

2.4.1. Cell culture

Human U937 monocytic cells were obtained from the American Tissue Culture Collection (Manassas, VA) and maintained in RPMI 1640 medium containing 10% fetal bovine serum (Gemini, Woodland, CA), 100 U penicillin, and 100 μg/mL streptomycin supplemented with 4.5 g/L glucose, and 1 mM sodium pyruvate. Cell cultures were maintained at cell concentrations between 2 × 105-2 × 106 cells/mL. For differentiation into macrophages, U937 cells were treated with 12-0-tetradecanoyl-phorbol-13-acetate (TPA; 3 μg/mL) and allowed to adhere for 48 h in a 5% CO2 tissue culture incubator at 37 °C, after which they were fed with TPA-free medium. Differentiation state was assessed by an attached cell phenotype and increased expression of MAC-2 (Castaneda et al., 2018b).

2.4.2. Cell exposure

Cells were exposed in triplicate by adding 10 μg/mL of phosphate-buffered saline (PBS; negative control), PM (ultrafine, $PM_{2.5}$ or PM_{10}), or LPS and FIZC (positive controls) directly to the media and incubating for 4 or 24 h. Each PM sample was sonicated for 25 min prior treatment to decrease agglomeration. The optimal dose was determined using a dose response curve (1 μg/mL, 2.5 μg/mL, 5 μg/mL, 10 μg/mL, 20 μg/mL, 50 μg/mL) for each PM size fraction. The dose of 10 μg/mL was found to induce a measurable response in the absence of detectable cell death for each size fraction with each of the biomarkers mentioned above.

2.4.3. Cell response

Total RNA was isolated from macrophages using a high-purity RNA isolation kit (ZymoResearch) and cDNA synthesis was performed as described previously (Vogel et al., 2005). Quantitative detection of housekeeping gene, β-actin, and differentially expressed genes (listed above) was performed with a LightCycler Instrument (LC480 Roche Diagnostics, Mannheim, Germany) using the QuantiTect Fast SYBR Green PCR Kit (Qiagen) according to the manufacturer's specifications. To confirm the amplification specificity, the PCR products were subjected to melting curve analysis.

2.4.4. Aryl hydrocarbon Receptor (AhR) Activity

Aryl hydrocarbon Receptor (AhR) Activity was measured using stably transfected HepG2 cells seeded at a density of 1.2×10^4 cells/well onto 24 well plates in DMEM media (Gibco Life Technologies, Grand Island, NY). HepG2 cells are stable transfected with PTX.DIR containing a DRE luciferase reporter construct as described elsewhere (Castaneda et al., 2018a). PTX.DIR consists of two xenobiotic response element sequences extending from nucleotides −1026 to −999 relative to the transcription start site of the rat CYP1A1 gene and inserted in a vector containing the herpes simplex virus thymidine kinase promoter and the luciferase reporter gene. Cells were then treated in triplicate with negative control (nanopure water), PM (ultrafine, $PM_{2.5}$ or PM_{10}), or positive control TPA (2-O-tetradecanoylphorbol-13-acetate; 5 μg/mL) and incubated for 4 h. AhR activity was measured with the luciferase reporter assay system (Promega Corp., Madison, WI) according to the manufacturer's instructions. Chemiluminescence was measured using 20 μL of cell lysate and a luminometer (Berthold Lumat LB 9501/16, Pittsburg, PA). Data is expressed as relative light units (RLU).

2.5. Statistical Analysis

Data are expressed as the mean±standard error of the mean (SEM). Gene expression data are normalized to control as well as to the expression level of the housekeeping gene, β-actin, with inter-group comparisons using two-way ANOVA followed by Tukey's multiple comparison test using GraphPad Prism 8 software. A value of $p < 0.05$ was considered statistically significant. Correlations of peaks in HRMS to in-vitro outcomes were performed as previously described, using custom scripts based on Matlab's linear regression model (Chan LK, 2020.). Furthermore, statistical methods such as Positive Matrix Factorization (PMF) were applied to the acquired HRAMS mass spectra to explore how concentrations of different analytes and classes of species vary with respect to each other and to quantitatively determine the contributions

of different sources to air pollutants in different samples (Sun et al., 2011; Zhang et al., 2011).

3. Results

Meteorological Data: Wind speed and direction data from the sampling period is depicted in Fig. 2 as a polar graph showing the natural logarithm of the frequency of observation for wind speeds greater than 2 m/s as a function of wind direction. It is overlaid on a Google map of the Imperial Valley centered about the sampling site on the Calipatria School District campus. Although these data indicate that the winds predominantly originate from the south and southwest during this study, which is the direction of Mexicali, there are also significant wind events originating from the direction of the Salton Sea. As a result, the PM samples collected during this study are considered to be a mixture of emissions from Mexicali, the Salton Sea playa, surrounding agricultural and livestock operations, as well as local residential activities such as cooking and driving.

Chemical Characterization: Results from the HRAMS indicate that organic species dominate Imperial Valley PM in every size fraction (Fig. 3). The distribution of the ionic fragments from electron-ionization of organic species (depicted in the second and third column of Fig. 3) is highly complex, suggesting the PM is likely composed of hundreds of carbon-containing compounds. Further molecular composition analysis of the organic fraction with LTQ-Orbitrap HRMS confirmed the presence of hundreds of individual molecules in each size fraction, and showed amines and sulfuric acid are much higher in the ultrafine fraction than in $PM_{2.5}$ and PM_{10} (data not shown). Hydrocarbons and oxygenated hydrocarbons however, follow an opposite trend, increasing in percentage with particle size (ultrafine, 15%; $PM_{2.5}$, 60%; PM_{10}, 64%). The majority of metals measured via ICPMS were salts and crustal materials (Ca, Na; Al, Fe, Mg & Si) (Fig. 4). This high percentage of crustal material in PM_{10} was also observed via SEM of the PM-coated substrate (Supplemental Table 2). In a recent paper by Snider et al., authors used a Zn:Al ratio to quantify anthropogenic versus natural sources (Snider et al., 2016). In Imperial Valley PM, the Zn:Al ratio decreased as particle size increased, suggesting more anthropogenic contributions to ultrafine PM, and a PM_{10} fraction dominated by crustal material and regional dust.

Endotoxin and ß-glucan quantification: Heat treatment of ultrafine and $PM_{2.5}$ samples resulted in significantly less endotoxin and β-glucan than the unheated samples (Fig. 5). However, heat-treatment of PM_{10} samples did not reduce the amount of detectable bioaerosol for either endotoxin or β-glucan. Significant differences in the presence of the bioaerosols were observed before and after heating, as well as between size fractions in the heated and unheated aliquots.

Gene Expression: The biological response to the three PM size fractions was significantly different depending on PM size, the specific gene measured and exposure time (Fig. 6). During the 24-h incubation (Fig. 6a), ultrafine and $PM_{2.5}$ significantly increased gene expression of *CYP1a1* compared to PM_{10} and the negative control (PBS). $PM_{2.5}$ also significantly increased expression of *CXCL2* and *IL-1β* compared to the negative control. PM_{10} significantly increased expression of all inflammatory markers. Expression of *HO-1* showed no significant changes between groups, while also showing a high crossing point during analysis, suggesting the possibility that this gene cannot be readily measured in U937 cells. Results from exposure to aliquots heated overnight at

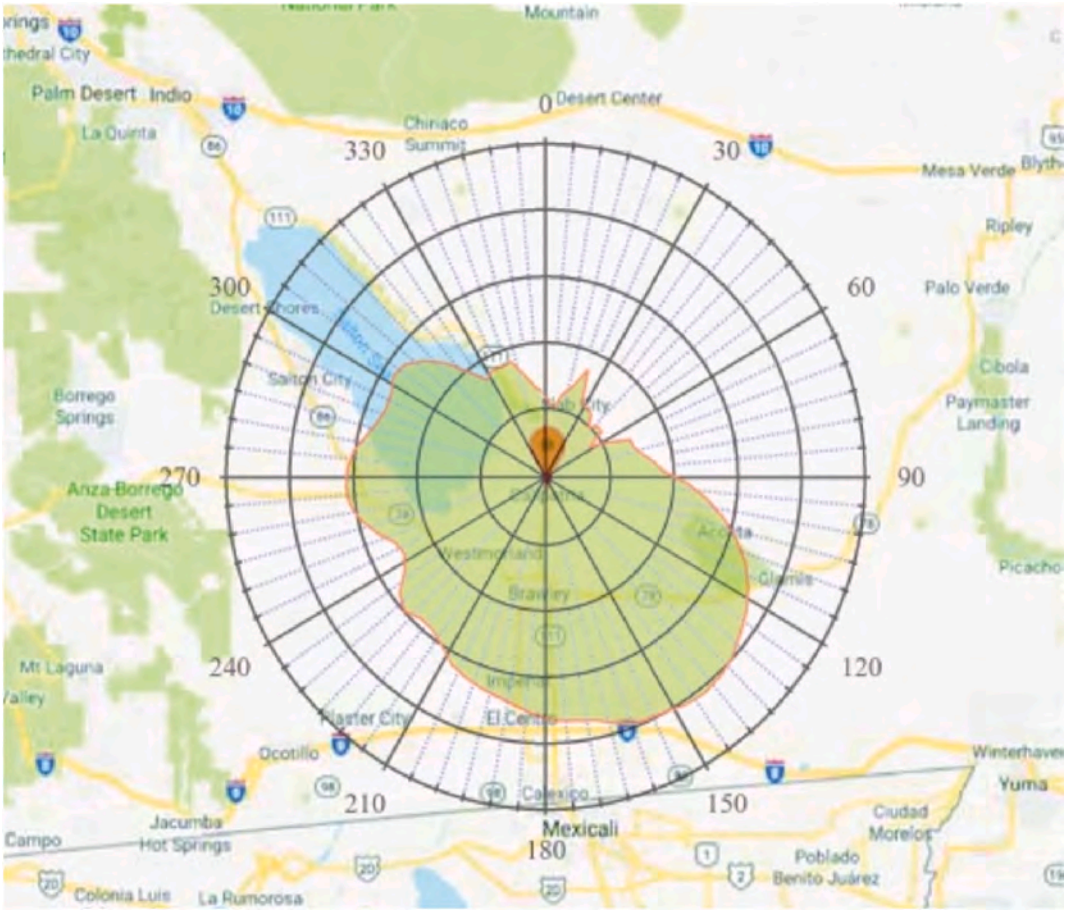

Fig. 2. The natural logarithm of the frequency of observation for wind speeds greater than 2 m/s as a function of wind direction is depicted in a polar graph and overlaid on a map of the Imperial Valley centered about Calipatria. These data were obtained from the PMSAMP deployed on the Calipatria School District campus during this study. Wind direction is reported in degrees clockwise from true north.

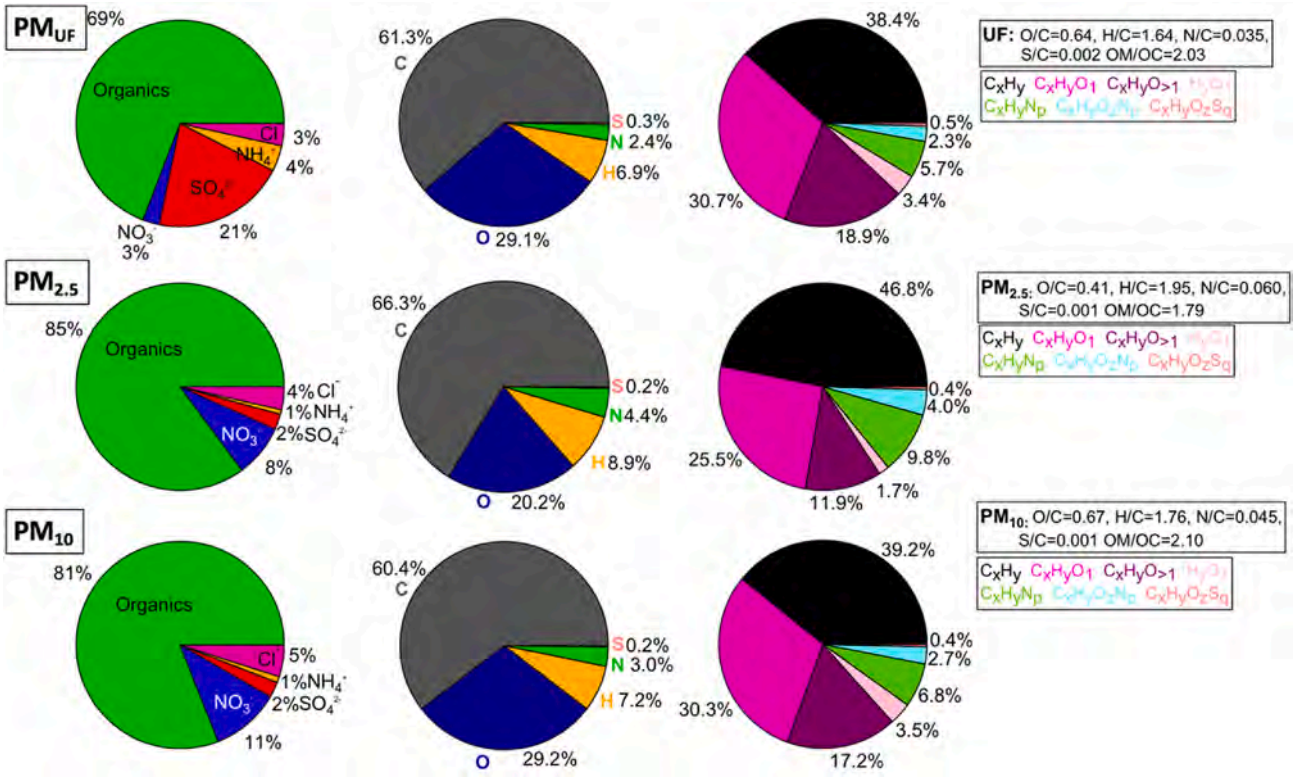

Fig. 3. High-resolution time-of-flight aerosol mass spectrometry (HRAMS) results for three size fractions of PM: ultrafine (PM_{UF}; top row), fine ($PM_{2.5}$; second row), coarse (PM_{10}; bottom row). The first column of pie graphs is the breakdown of organic versus inorganic compounds. The second column of pie graphs is the elemental breakdown of the organic fraction. The third pie graph depicts the percentage of each compound listed in the far-right legend.

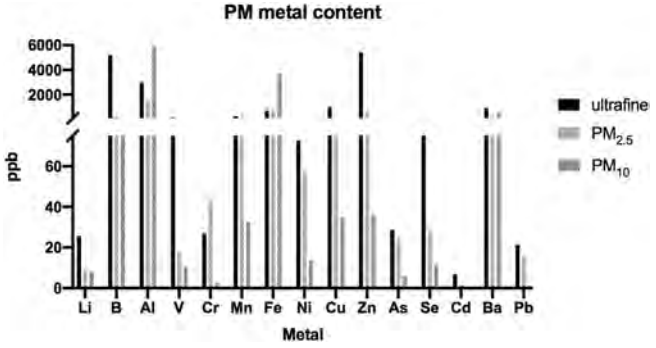

Fig. 4. Inductively Coupled Plasma-Mass Spectrometry (ICP-MS) results for trace metals in ultrafine, $PM_{2.5}$ and PM_{10} samples. Concentrations are reported as metal concentration detected in 1000 ppb of PM sample.

120 °C demonstrated that heating PM_{10} samples significantly changed the biological response. There was no significant difference in expression levels between the heated and unheated samples of ultrafine and $PM_{2.5}$.

During the 4-h incubation (Fig. 6b), ultrafine and $PM_{2.5}$ significantly increased gene expression of *CYP1a1* compared to the negative control (PBS) or PM_{10}. $PM_{2.5}$ also significantly increased expression of *CXCL2* and *IL-6* compared to the negative control. PM_{10} significantly increased expression of *CXCL2, IL-1β, IL-8* and *IL-6*. These patterns differ slightly from the biological response measured after 24-h of incubation. However, the timepoints were not compared statistically since the experiments were run on different dates.

AhR Activity: Polycyclic aromatic hydrocarbons in PM are one of many compounds that activate the AhR in bronchial epithelial cells (Harmon et al., 2018a). In this experiment, HepG2 cells were used to measure AhR activity due to their higher transfection efficiency. Results demonstrated that after 4 h of incubation, AhR activity was significantly higher following exposure to ultrafine and $PM_{2.5}$ compared to PM_{10} or the negative PBS control (Fig. 7).

Correlations: As PM size increases, expression of CYP1A1 decreases and expression of all other measured biomarkers *(COX-2, IL-1β, IL-6, IL-8, IL-10, CXCL2)* increases. This data was analyzed with the HRMS chemical analysis to look for correlations between the biological endpoint of gene expression and the presence of organic compounds within each size fraction. In addition, we examined the potential correlation between metal content and biological response. Positive correlations were observed between Thallium, Iron and all inflammatory markers (*COX-2, IL-1β, IL-6, IL-8, IL-10, CXCL2)* and a negative correlation was observed between Arsenic and *IL-6*. However, for the metal analysis there were no size replicates (only three points – ultrafine, $PM_{2.5}$ and PM_{10} – to correlate), so results should be interpreted with caution.

4. Discussion

Throughout the United States, $PM_{2.5}$ and PM_{10} levels are tracked through networks of regulatory air monitors. These monitoring devices collect particle counts which are converted to mass and an air quality index (AQI) which designates a risk-level and provides health recommendations for residents (AirNow.gov, 2019). National and state air quality standards are set as mass limits ($\mu g/m^3$) for daily and national averages. In addition to the national regulatory monitors, Imperial Valley has a local network of 50 monitors, maintained through the IVAN (Identifying Violations Affecting Neighborhoods) program to track real-time air quality for $PM_{2.5}$ and PM_{10} (IVAN, 2019). These data, as well as the national air quality standards, do not account for any differences in particle composition. Due to the wide variety of PM sources throughout Imperial Valley and the differences in physiochemical

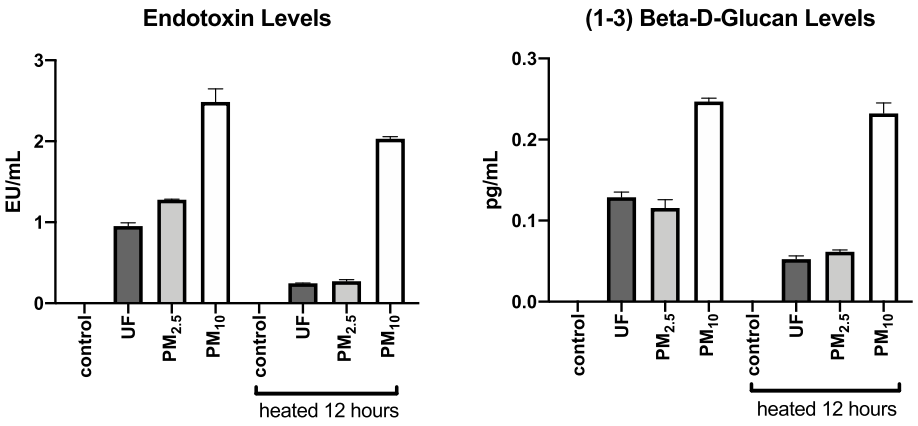

Fig. 5. Endotoxin and β-glucan levels were measured in two aliquots of each size fraction of PM. One aliquot was heated overnight at 120 °C. All groups (heated and unheated) are significantly higher than blank control. Ultrafine and fine size fractions are significantly different from size-matched heat group using a one-way ANOVA and Tukey's multiple comparisons test. p value (<0.05).

composition of and biological response to each size fraction, more than mass data should be considered when determining health recommendations.

Wind data collected during the PM sampling period demonstrated the majority of wind events originating from the south to southwest, which is in the direction of Mexicali, with significant wind events from the direction of the Salton Sea as well. Additional wind data not reported here show strong seasonality to both wind speed and direction, including: *(1)* more frequent and stronger wind events in the fall and spring, *(2)* predominantly westerlies and north-westerlies originating from the direction of the Salton Sea during winter and spring, and *(3)* wind events distributed relatively evenly between originating from the south (Mexicali) and northwest (Salton Sea) in fall. This data could be useful to residents by informing them of the timing and duration of wind-induced pollution episodes and the likely sources contributing to those events, as well as acute exposures to obvious PM sources such as agricultural burns and dust storms. Smaller particles are likely to travel longer distances, whereas larger particles are affected more by gravity, and thus do not remain in the atmosphere as long (Fuzzi et al., 2015; Kozawa et al., 1994). However, small particles have diffusive loss, and thus, depending on ground surface and weather, there is a diameter of slowest deposition between very large and very small particles (Zhang et al., 2001). A review by Fuzzi et al. (2015) describes how particles evolve continuously, becoming more homogenous via atmospheric processing as they travel further from their sources (Fuzzi et al., 2015). Limitations of offsite analyses of PM are 1) the incomplete and differential extraction of particles from the collection substrates, 2) the agglomeration of particles on the collection substrate that do not allow for individual particle separation and 3) a certain degree of particle transformation during the collection and extraction process. Since extracted particles are used to measure biological responses, these may not completely reflect real-time exposure to ambient airborne particles.

Based on the compositional analyses corroborated by both HRMS, HRAMS, and ICPMS, each size fraction of PM collected and extracted was compositionally different. All size fractions were dominated by organics, but the secondary inorganic components varied. Ultrafine PM contained a significantly higher percentage of sulfates, suggesting the presence of coal burning which emits significant amounts of SO_2. Formation and growth of new particles from SO_2 oxidation was likely an important process forming ultrafine sulfate. Indeed, the low measurement of NH_4^+ ions in ultrafine particles (Fig. 3) indicates that they are acidic. As SO_2 can be transported great distances, it is possible that elevated sulfate levels in ultrafine particles are due to combustion processes in Mexicali or other locations across the border (Kelly et al., 1995). Data from Mendoza et al. corroborate this finding with high sulfate measurements in $PM_{2.5}$ collected specifically from Mexicali (Mendoza et al., 1995). $PM_{2.5}$ collected from the northern part of Imperial Valley has significantly lower sulfates than in the ultrafine PM, suggesting a different, local, source for these $PM_{2.5}$ samples.

None of the PM exposures had a significant impact on cell viability in macrophages (Supplemental Figure 2). This finding demonstrates the biological response was not due to cell death at the tested concentrations. The response measured via gene expression was significant between PM-exposed cells and control filter exposures, as well as between smaller and larger particles. PM exposure for 24 h demonstrated that the larger size fraction, PM_{10}, invoked more of an inflammatory response, whereas the smaller particles, $PM_{2.5}$ and ultrafine PM, only increased *CYP1a1* expression. Oxidative stress responses to $PM_{2.5}$ have been measured in many locations and environments, especially when combustion particles, and thus PAHs, are present (Harmon et al., 2018b; Liu et al., 2008; Lodovici and Bigagli, 2011). In the Imperial Valley, the idling of vehicles at the border crossing, local traffic patterns, and agricultural vehicles throughout the Valley produce combustion particles that could be involved in this response (Kelly et al., 1995). Additional trends between the biological response and chemical composition data were observed with a correlation analysis. Increases in *CYP1a1* (smaller particles) correlated with an increase in aliphatic amines whereas increases in all inflammatory markers (*COX-2, IL-1β, IL-6, IL-8, IL-10, CXCL2;* larger particles) correlate with increases in hydrocarbons and heterocyclic nitrogen.

To further elucidate the mechanism of the observed biological response when exposed to Imperial Valley PM, activation of AhR was measured. AhR has been shown to be involved in both oxidative stress and inflammatory responses in lungs; and although CYP1a1 is the only AhR-dependent gene, inflammatory markers *IL-1*, *IL-6* and *IL-8*, are activated further down in the AhR cascade (Attafi et al., 2019; Castaneda et al., 2018b; Nebert et al., 2004; Vogel et al., 2007). Data from the luciferase assay 4 h post-exposure demonstrated that only $PM_{2.5}$ and ultrafine particles activate AhR. This data is consistent with previous research that shows an activation of AhR with exposure to $PM_{2.5}$ (Castaneda et al., 2018b). These results indicate that the inflammatory response observed via increases in *IL-1 β*, *IL-6* and *IL-8* with the PM_{10} exposure at 4- and 24-h post-exposure was not mediated through AhR. Ultrafine particles possess more AhR activating chemicals which are also more bioavailable to bind to the AhR in the cytosol to induce CYP1a1. This activation of intracellular AhR by ultrafine PM leads us to predict these particles have an effect by internalization into cells. For larger PM_{10} particles, although also possibly internalized into cells, activation of other pathways such as nuclear factor κB (NF-κB), also allows for the possibility that components of PM_{10} may act directly as a ligand to activate upstream membrane-bound receptors (Silbajoris et al., 2011). However, in several studies *CYP1a1 a*ctivity has been shown to be

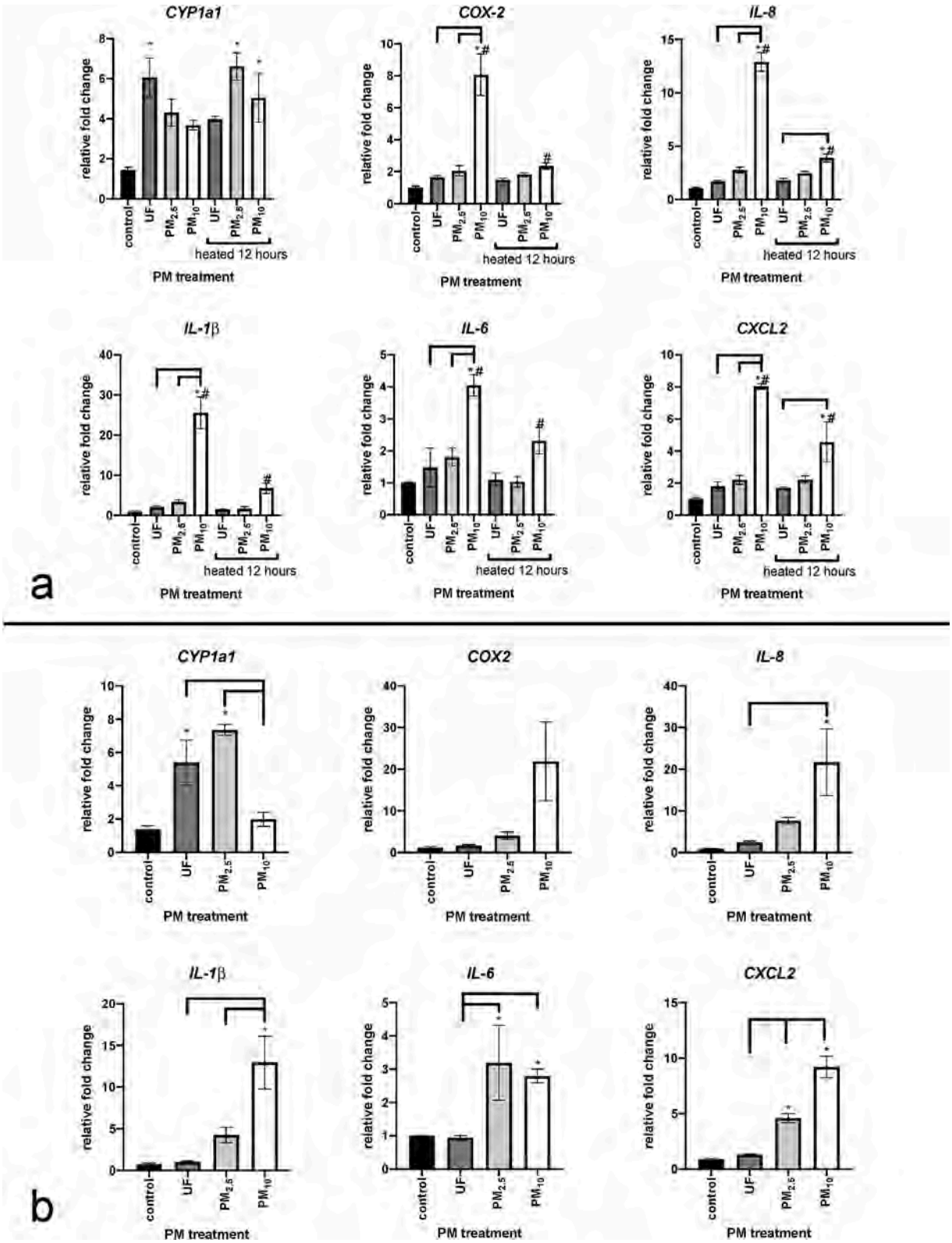

Fig. 6. *Biological response of U937 macrophages after 24-h (A) and 4-h (B) exposure to* 10 μg/mL *of heated or unheated PM (ex: ultrafine h = heated overnight at 120 °C). Response was measured in gene expression calculated as relative fold change from control. (*) indicates significance from control, (#) indicates significance from size-matched heat treatment, and brackets indicate significance between groups, calculated using a One-way ANOVA and Tukey's multiple comparisons test at p value (< 0.05).*

decreased in animals exposed to endotoxin (LPS)-treated mice (Arlt et al., 2015; Ke et al., 2001; Wu et al., 2011). Arlt et al. determined this decrease was due to inflammation acting as a deterrent for bioactivation and detoxification. The high levels of endotoxin measured in Imperial Valley PM_{10}, as well as the observed increase of inflammatory cytokines, could be another explanation for low *CYP1a1* expression and low AhR activity with PM_{10} exposure.

PM_{10} fractions typically contain bioaerosols such as endotoxin that

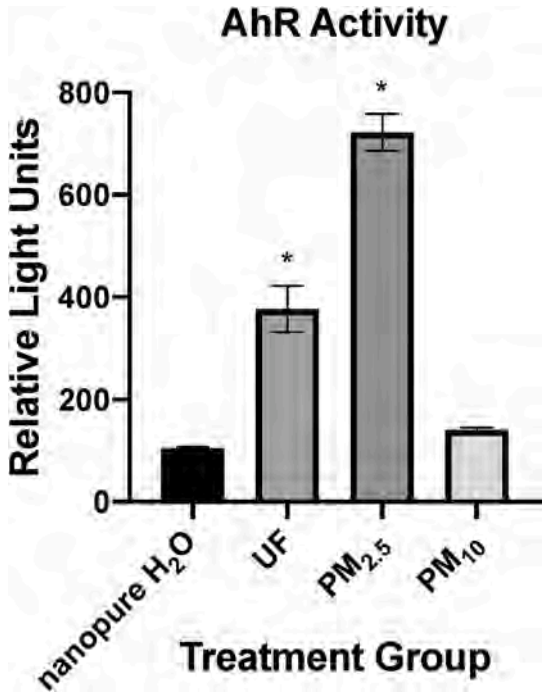

Fig. 7. Aryl-hydrocarbon receptor activity measured in relative light units with a Luciferase reporter assay. (*) indicates significance from control calculated using a One-way ANOVA at p value (<0.05).

have the ability to invoke an inflammatory response through non-AhR mediated pathways (such as via toll-like receptor 4 (TLR4)) (Cavaillon, 2018; Kirkhorn and Garry, 2000; Shoenfelt et al., 2009). As previously mentioned, PM_{10} samples from Imperial Valley had significantly higher levels of endotoxin than $PM_{2.5}$ and ultrafine PM. Although the physical size of endotoxin itself is small (Bergstrand et al. measured LPS aggregates with TEM of up to 9–19 nm), the tendency to agglomerate with larger, PM_{10} particles (instead of to smaller particles) has been observed throughout the literature (Bergstrand et al., 2006; Heinrich et al., 2003; Pavilonis et al., 2013). In Imperial Valley, endotoxin in the PM is likely due to the presence of three large cattle feedlots located north and south of the sampling site (Johnston et al., 2019; Wilson et al., 2002). To determine if the presence of endotoxin was contributing to the inflammatory response observed *in vitro,* PM samples were heated overnight in an attempt to remove the bioaerosol. Heating, in addition to blocking with polymyxin B (data not show), was not effective in removing endotoxin from the PM_{10} samples. Nevertheless, when macrophages were exposed to these heated PM_{10} samples, the inflammatory response was significantly reduced. As the concentration of endotoxin was not reduced, this data indicates that it is not endotoxin, but rather a different component of the PM_{10} that is responsible for the observed inflammatory response. This finding demonstrates a unique feature of Imperial Valley PM_{10}, as it is in contrast to findings by Shoenfelt et al. (2009) and others that demonstrated a strong influence of endotoxin in the inflammatory response to PM_{10} (Adar et al., 2015; Shoenfelt et al., 2009). We hypothesize that a compound within the organic fraction of PM, or an unidentified bioaerosol within this size fraction was inactivated during heating.

5. Conclusion

Particle size has a clear and strong influence on biological response (Cho et al., 2009; Dick et al., 2003; Gilmour et al., 2007). In Imperial Valley and elsewhere, health effects of PM should not be assumed to be due to one size fraction. Although particles agglomerate, homogenize and chemically evolve as they move through the atmosphere, particle composition remains significantly different between size fractions. This fact, as well as our biological response data, suggest that the mechanisms of inflammation and toxicity are distinct between size fractions due to their chemical composition. Ambient PM collected from a single region can demonstrate distinct mechanistic responses based on particle source. Although further data is needed, this *in vitro* study begins to elucidate distinct mechanisms of the biological response to differing PM sizes and thus sources in Imperial Valley, California.

Funding

This work was supported by the National Institute for Occupational Safety and Health (NIOSH) grants U54 OH07550 and U01 OH010969 and the National Institute of Environmental Health Sciences (NIEHS) grants R01 ES025229, P30 ES023513, and P51 OD011107. S.M.D. was supported by NIEHS T32 ES007059, T32 HL007013 and NIEHS T32ES015459. This work was supportd in part by the Biostatistics, Epidemiologic and Bioinformatic Training in Environmental Health (BEBTEH) Training Grant, Grant #: NIEHS T32ES015459.

CRediT authorship contribution statement

S.M. D'Evelyn: Conceptualization, Methodology, Formal analysis, Investigation, Writing - original draft, Visualization, Project administration. **Vogel CFA:** Conceptualization, Methodology, Resources, Supervision. **Bein KJ:** Software, Investigation, Resources. **Lara B:** Methodology, Investigation, Visualization. **Laing EA:** Investigation. **Abarca RA:** Investigation. **Zhang Q:** Investigation, Resources, Writing - review & editing, Visualization. **Li L:** Investigation. **Li J:** Investigation. **Nguyen TB:** Formal analysis, Investigation, Resources, Writing - review & editing. **Pinkerton KE:** Conceptualization, Methodology, Writing - review & editing, Supervision, Funding acquisition.

Declaration of competing interest

The authors declare that they have no known competing financial interests or personal relationships that could have appeared to influence the work reported in this paper.

Acknowledgements

We would like to thank Dale Uyeminami, Sheccid Torres and Sarah Kado for their laboratory assistance, as well as Humberto Lugo and Comite Civico del Valle for their help engaging the community and in selecting the collection site.

Appendix A. Supplementary data

Supplementary data to this article can be found online at https://doi.org/10.1016/j.atmosenv.2020.117992.

References

Adar, S.D., et al., 2015. "Markers of inflammation and coagulation after long-term exposure to coarse particulate matter: a cross-sectional analysis from the multi-ethnic study of atherosclerosis.". Environ. Health Perspect. 123 (6), 541–548.

Aiken, A.C., DeCarlo, P.F., Jimenez, J.L., 2007. Elemental analysis of organic species with electron ionization high-resolution mass spectrometry. Analytical Chemistry.

Aiken, A.C., DeCarlo, P.F., Kroll, J.H., Worsnop, D.R., Huffman, J.A., Docherty, K., Ulbrich, I.M., Mohr, C., Kimmel, J.R., Sueper, D., Sun, Y., Zhang, Q., Trimborn, A., Northway, M., Ziemann, P.J., Canagaratna, M.R., Onasch, T.B., Alfarra, M.R., Prevot, A.S.H., Dommen, J., Duplissy, J., Metzger, A., Baltensperger, U., Jimenez, J. L., 2008. O/C and OM/OC ratios of primary, secondary, and ambient organic aerosols with a high resolution time-of-flight aerosol mass spectrometer. Environ. Sci. Technol. 42, 4478–4485.

AirNowgov, 2019. Environmental protection agency, airnow.gov. Air Quality Index (AQI) Basics.

American Lung Association, 2019. The state of the air. American lung association, lung.org.

Arlt, V.M., Krais, A.M., Godschalk, R.W., Riffo-Vasquez, Y., Mrizova, I., Roufosse, C.A., Corbin, C., Shi, Q., Frei, E., Stiborova, M., van Schooten, F.-J., Phillips, D.H., Spina, D., 2015. Pulmonary inflammation impacts on CYP1A1-mediated respiratory tract DNA damage induced by the carcinogenic air pollutant benzo[a]pyrene. Toxicological sciences. an official journal of the Society of Toxicology 146, 213–225.

Attafi, I.M., Albakheet, S.A., Korashy, H.M., 2019. The role of NF-κB and AHR transcription factors in lead-induced lung toxicity in human lung cancer A549 cells. Toxicol. Mech. Methods 1–32.

Badirdast, P., Rezazadeh Azari, M., Salehpour, S., Ghadjari, A., Khodakarim, S., Panahi, D., Fadaei, M., Rahimi, A., 2017. The effect of wood aerosols and bioaerosols on the respiratory systems of wood manufacturing industry workers in golestan province. Tanaffos 16, 53–59.

Bein, K.J., Wexler, A.S., 2014. A high-efficiency, low-bias method for extracting particulate matter from filter and impactor substrates. Atmos. Environ. 90, 87–95.

Bergstrand, A., Svanberg, C., Langton, M., Nydén, M., 2006. Aggregation behavior and size of lipopolysaccharide from Escherichia coli O55:B5. Colloids Surf. B Biointerfaces 53, 9–14.

California Air Resources Board, October 2018. 2018. Imperial county 2018 REDESIGNATION request and maintenance plan for particulate matter less than 10 microns IN diameter. In: District, A.P.C. (Ed.), Ramboll US Corporation. Imperial County, California.

Canagaratna, M., Jayne, J., Jimenez, J.L., Allan, J.A., Alfarra, R., Zhang, Q., Onasch, T., Drewnick, F., Coe, H., Middlebrook, A., Delia, A., Williams, L., Trimborn, A., Northway, M., DeCarlo, P., Kolb, C., Davidovits, P., Worsnop, D., 2007. Chemical and microphysical characterization of ambient aerosols with the aerodyne aerosol mass spectrometer. DOI:110.1002/mas.20115 Mass Spectrom. Rev. 26, 185–222.

Castaneda, A.R., Pinkerton, K.E., Bein, K.J., Magana-Mendez, A., Yang, H.T., Ashwood, P., Vogel, C.F.A., 2018a. Ambient particulate matter activates the aryl hydrocarbon receptor in dendritic cells and enhances Th17 polarization. Toxicol. Lett. 292, 85–96.

Castaneda, A.R., Vogel, C.F.A., Bein, K.J., Hughes, H.K., Smiley-Jewell, S., Pinkerton, K. E., 2018b. Ambient particulate matter enhances the pulmonary allergic immune response to house dust mite in a BALB/c mouse model by augmenting Th2- and Th17-immune responses. Physiological reports 6, e13827.

Cavaillon, J.M., 2018. Exotoxins and endotoxins: inducers of inflammatory cytokines. Toxicon. official journal of the International Society on Toxinology 149, 45–53.

Chan, L.K., Karim N, N.K., Yang, Y., Rice, R.H., He, G., Denison, M.S., Nguyen, T.B., 2020. Relationship between the molecular composition, visible light absorption, and health-related properties of smoldering woodsmoke aerosols. Atmos Chem Phys. Accepted.

Cho, S.-H., et al., 2009. Comparative toxicity of size-fractionated airborne particulate matter collected at different distances from an urban highway. Environ. Health Perspect. 117 (11), 1682–1689.

DeCarlo, P.F., Kimmel, J.R., Trimborn, A., Jayne, J., Aiken, A.C., Gonin, M., Fuhrer, K., Horvath, T., Worsnop, D.R., Jimenez, J.L., 2006. A field-deployable high-resolution time-of-flight aerosol mass spectrometer. Analytical chemistry.

Demokritou, P., Kavouras, I.G., Ferguson, S.T., Koutrakis, P., 2002. Development of a high volume cascade impactor for toxicological and chemical characterization studies. Aerosol. Sci. Technol. 36, 925–933.

Dick, C.A.J., et al., 2003. "Murine pulmonary inflammatory responses following instillation of size-fractionated ambient particulate matter.". J. Toxicol. Environ. Health, Part A 66 (23), 2193–2207.

Douwes, J., 2005. (1–>3)-Beta-D-glucans and respiratory health: a review of the scientific evidence. Indoor Air 15, 160–169.

Frie, A.L., Dingle, J.H., Ying, S.C., Bahreini, R., 2017. The effect of a receding saline lake (the Salton Sea) on airborne particulate matter composition. Environ. Sci. Technol. 51, 8283–8292.

Fuzzi, S., Baltensperger, U., Carslaw, K., Decesari, S., Denier van der Gon, H., Facchini, M.C., Fowler, D., Koren, I., Langford, B., Lohmann, U., Nemitz, E., Pandis, S., Riipinen, I., Rudich, Y., Schaap, M., Slowik, J.G., Spracklen, D.V., Vignati, E., Wild, M., Williams, M., Gilardoni, S., 2015. Particulate matter, air quality and climate: lessons learned and future needs. Atmos. Chem. Phys. 15, 8217–8299.

Ge, X., Shaw, S., Zhang, Q., 2014. Toward understanding amines and their degradation products from post-combustion CO_2 capture processes with aerosol mass spectrometry. Environ. Sci.. and Technol. 48, 5066–5075.

Gilmour, M.I., et al., 2007. "Comparative toxicity of size-fractionated airborne particulate matter obtained from different cities in the United States.". Inhal Toxicol 19 Suppl 1, 7–16.

Harmon, A.C., Hebert, V.Y., Cormier, S.A., Subramanian, B., Reed, J.R., Backes, W.L., Dugas, T.R., 2018a. Particulate matter containing environmentally persistent free radicals induces AhR-dependent cytokine and reactive oxygen species production in human bronchial epithelial cells. PloS one 13, e0205412.

Harmon, A.C., Hebert, V.Y., Cormier, S.A., Subramanian, B., Reed, J.R., Backes, W.L., Dugas, T.R., 2018b. Particulate matter containing environmentally persistent free radicals induces AhR-dependent cytokine and reactive oxygen species production in human bronchial epithelial cells. PloS One 13, e0205412.

Health, C.D.o.P., 2015-2017. CA department of Public Health, CA.gov. California Breathing: County Asthma Data Tool.

Heinrich, J., Pitz, M., Bischof, W., Krug, N., Borm, P.J.A., 2003. Endotoxin in fine (PM2.5) and coarse (PM2.5–10) particle mass of ambient aerosols. A temporo-spatial analysis. Atmos. Environ. 37, 3659–3667.

IVAN, 2019. In: Comite Civico del Valle, I. (Ed.), Identifying Violations affecting Neighborhoods: imperial. IVAN Imperial.

Johnston, J.E., et al., 2019. The disappearing Salton Sea: a critical reflection on the emerging environmental threat of disappearing saline lakes and potential impacts on children's health.". Sci. Total Environ. 663, 804–817.

Ke, S., Rabson, A.B., Germino, J.F., Gallo, M.A., Tian, Y., 2001. Mechanism of suppression of cytochrome P-450 1A1 expression by tumor necrosis factor-alpha and lipopolysaccharide. J. Biol. Chem. 276 (43), 39638–39644. https://doi.org/10.1074/jbc.M106286200.

Kelly, F.J., Fussell, J.C., 2012. Size, source and chemical composition as determinants of toxicity attributable to ambient particulate matter. Atmos. Environ. 60, 504–526.

Kelly, K., Wagner, D., Lighty, J., Quintero Nunez, M., Vazquez, F.A., Collins, K., Barud-Zubillaga, A., 1995. 2006. Black carbon and polycyclic aromatic hydrocarbon emissions from vehicles in the United States-Mexico border region: pilot study. J. Air Waste Manag. Assoc. 56, 285–293.

Kelly, K.E., Jaramillo, I.C., Quintero-Nunez, M., Wagner, D.A., Collins, K., Meuzelaar, H. L., Lighty, J.S., 1995. 2010. Low-wind/high particulate matter episodes in the Calexico/Mexicali region. J. Air Waste Manag. Assoc. 60, 1476–1486.

Kendrick, E., 1963. A mass scale based on CH2 = 14.0000 for high resolution mass spectrometry of organic compounds. Anal. Chem. 35, 2146–2154.

Kind, T., Fiehn, O., 2007. Seven Golden Rules for heuristic filtering of molecular formulas obtained by accurate mass spectrometry. BMC Bioinf. 8, 105.

Kirkhorn, S.R., Garry, V.F., 2000. Agricultural lung diseases. Environ. Health Perspect. 108 (Suppl. 4), 705–712.

Kozawa, K.H., Winer, A.M., Fruin, S.A., 1994. 2012. Ultrafine particle size distributions near freeways: effects of differing wind directions on exposure. Atmos. Environ. 63, 250–260.

Lingappan, K., Maity, S., Jiang, W., Wang, L., Couroucli, X., Veith, A., Zhou, G., Coarfa, C., Moorthy, B., 2017. Role of cytochrome P450 (CYP)1A in hyperoxic lung injury: analysis of the transcriptome and proteome. Sci. Rep. 7, 642.

Liu, G., Niu, Z., Van Niekerk, D., Xue, J., Zheng, L., 2008. Polycyclic aromatic hydrocarbons (PAHs) from coal combustion: emissions, analysis, and toxicology. Rev. Environ. Contam. Toxicol. 192, 1–28.

Lodovici, M., Bigagli, E., 2011. Oxidative stress and air pollution exposure. J. Toxicol. 2011, 487074.

Mack, S.M., Madl, A.K., Pinkerton, K.E., 2019. Respiratory health effects of exposure to ambient particulate matter and bioaerosols. Comprehensive physiology. 10.1002/cphy.c180040.

Madl, A.K., Carosino, C., Pinkerton, K.E., 2010. 8.22-Particle Toxicities. In: McQueen, C. A. (Ed.), Comprehensive Toxicology, second ed. Elsevier, Oxford, pp. 421–451.

Mendoza, A., Pardo, E.I., Gutierrez, A.A., 1995. 2010. Chemical characterization and preliminary source contribution of fine particulate matter in the Mexicali/Imperial Valley border area. J. Air Waste Manag. Assoc. 60, 258–270.

Nebert, D.W., Dalton, T.P., Okey, A.B., Gonzalez, F.J., 2004. Role of aryl hydrocarbon receptor-mediated induction of the CYP1 enzymes in environmental toxicity and cancer. J. Biol. Chem. 279, 23847–23850.

Parworth, C.L., Young, D.E., Kim, H., Zhang, X., Cappa, C.D., Collier, S., Zhang, Q., 2017. Wintertime water-soluble aerosol composition and particle water content in Fresno, California. J. Geophys. Res.: Atmosphere 122, 3155–3170.

Pavilonis, B.T., Anthony, T.R., O'Shaughnessy, P.T., Humann, M.J., Merchant, J.A., Moore, G., Thorne, P.S., Weisel, C.P., Sanderson, W.T., 2013. Indoor and outdoor particulate matter and endotoxin concentrations in an intensely agricultural county. J. Expo. Sci. Environ. Epidemiol. 23, 299–305.

Robertson, S., Douglas, P., Jarvis, D., Marczylo, E., 2019. Bioaerosol exposure from composting facilities and health outcomes in workers and in the community: a systematic review update. Int. J. Hyg Environ. Health 222, 364–386.

Samake, A., Uzu, G., Martins, J.M.F., Calas, A., Vince, E., Parat, S., Jaffrezo, J.L., 2017. The unexpected role of bioaerosols in the Oxidative Potential of PM. Sci. Rep. 7, 10978.

Shoenfelt, J., Mitkus, R.J., Zeisler, R., Spatz, R.O., Powell, J., Fenton, M.J., Squibb, K.A., Medvedev, A.E., 2009. Involvement of TLR2 and TLR4 in inflammatory immune responses induced by fine and coarse ambient air particulate matter. J. Leukoc. Biol. 86, 303–312.

Silbajoris, R., Osornio-Vargas, A.R., Simmons, S.O., Reed, W., Bromberg, P.A., Dailey, L. A., Samet, J.M., 2011. Ambient particulate matter induces interleukin-8 expression through an alternative NF-κB (nuclear factor-kappa B) mechanism in human airway epithelial cells. Environ. Health Perspect. 119, 1379–1383.

Snider, G., Weagle, C.L., Murdymootoo, K.K., Ring, A., Ritchie, Y., Stone, E., Walsh, A., Akoshile, C., Anh, N.X., Balasubramanian, R., Brook, J., Qonitan, F.D., Dong, J., Griffith, D., He, K., Holben, B.N., Kahn, R., Lagrosas, N., Lestari, P., Ma, Z., Misra, A., Norford, L.K., Quel, E.J., Salam, A., Schichtel, B., Segev, L., Tripathi, S., Wang, C., Yu, C., Zhang, Q., Zhang, Y., Brauer, M., Cohen, A., Gibson, M.D., Liu, Y., Martins, J. V., Rudich, Y., Martin, R.V., 2016. Variation in global chemical composition of PM2.5: emerging results from SPARTAN. Atmos. Chem. Phys. 16, 9629–9653.

Sun, Y., Zhang, Q., 2010. Bulk characterization and quantification of organic nitrogen species in atmospheric condensed phases based on high resolution time-of-flight Aerosol Mass Spectrometry. Environmental Science & Technology (in preparation).

Sun, Y., Zhang, Q., Zheng, M., Ding, X., Edgerton, E.S., Wang, X., 2011. Characterization and source apportionment of water-soluble organic matter in atmospheric fine particles ($PM_{2.5}$) with high-resolution aerosol mass spectrometry and GC-MS. Environ. Sci. Technol. 45, 4854–4861.

Vogel, C.F., Sciullo, E., Li, W., Wong, P., Lazennec, G., Matsumura, F., 2007. RelB, a new partner of aryl hydrocarbon receptor-mediated transcription. Mol. Endocrinol. 21, 2941–2955.

Vogel, C.F.A., Sciullo, E., Wong, P., Kuzmicky, P., Kado, N., Matsumura, F.D., 2005. Induction of proinflammatory cytokines and C-reactive protein in human macrophage cell line U937 exposed to air pollution particulates. Environ. Health Perspect. 113, 1536–1541.

Wegesser, T.C., Last, J.A., 2008. Lung response to coarse PM: bioassay in mice. Toxicol. Appl. Pharmacol. 230, 159–166.
Wilson, S.C., Morrow-Tesch, J., Straus, D.C., Cooley, J.D., Wong, W.C., Mitlöhner, F.M., McGlone, J.J., 2002. Airborne microbial flora in a cattle feedlot. Appl. Environ. Microbiol. 68, 3238.
Wu, D., Li, W., Lok, P., Matsumura, F., Vogel, C.F., 2011. AhR deficiency impairs expression of LPS-induced inflammatory genes in mice. Biochem. Biophys. Res. Commun. 410 (2), 358–363. https://doi.org/10.1016/j.bbrc.2011.06.018.
Zhang, L., Gong, S., Padro, J., Barrie, L., 2001. A size-segregated particle dry deposition scheme for an atmospheric aerosol module. Atmos. Environ. 35, 549–560.
Zhang, Q., Jimenez, J.L., Canagaratna, M., Ng, N.L., Ulbrich, I., Worsnop, D., Sun, Y.L., 2011. Understanding organic aerosols via factor Analysis of aerosol mass spectrometry: a review. Anal. Bioanal. Chem. 401, 3045–3067.